




Cite this: *Phys. Chem. Chem. Phys.*,  
2025, 27, 22894

Received 15th July 2025,  
Accepted 5th October 2025

DOI: 10.1039/d5cp02696b

rsc.li/pccp

# Cation distribution and its magnetic implications in gadolinium–iron garnets for an enhanced control of compensation temperature

Cristina Bartha, Claudiu Locovei, Andrei Alexandru-Dinu, Cezar Comanescu,  Mihai Alexandru Grigorescu, Andrei Kuncser, Nicusor Iacob, Magda Galatanu, Aurel Leca, Petre Badica \* and Victor Kuncser\*

The precise control of the magnetic compensation temperature ( $\theta_c$ ) in ferrimagnetic garnets is essential for the development of cutting-edge ultrafast customizable spintronic devices. In this work we demonstrate how fine variation in stoichiometry and cation distribution in iron gadolinium garnets significantly influences  $\theta_c$ . Two samples of  $\text{Gd}_3\text{Fe}_5\text{O}_{12}$  garnets synthesized via a new hydrothermal method and a conventional solid-state reaction, respectively, were considered. The complex study was carried out using a complex approach combining X-ray diffraction, magnetometry, and Mössbauer spectroscopy. Atomic-scale analysis revealed with unprecedented accuracy a cationic inversion between  $\text{Fe}^{3+}$  and  $\text{Gd}^{3+}$  at octahedral and dodecahedral sites in both samples, and their chemical compositions were determined as  $\text{Gd}_{2.70}\text{Fe}_{4.76}\text{O}_{11.9}$  and  $\text{Gd}_{2.96}\text{Fe}_{4.68}\text{O}_{11.5}$ , respectively. These local rearrangements have been shown to have a consistent influence on  $\theta_c$  (290 K and 317 K, respectively) around room temperature, emphasizing the high sensitivity of exchange interactions to internal atomic order. Results clearly illustrate the strong correlation between the processing, atomic configuration and macroscopic magnetic behavior, establishing a new paradigm for the design of garnet-based materials with tunable  $\theta_c$ . The strategy for the accurate determination of cation inversion illustrated in this work exhibits great potential in guiding material innovations for next-generation spintronics.

## 1. Introduction

Recent research in spintronic ultrafast spin storage devices has increasingly focused on ferrimagnetic rare-earth iron garnets with magnetization compensation properties. Among them,  $\text{Gd}_3\text{Fe}_5\text{O}_{12}$  (gadolinium iron garnet) is considered a promising candidate due to its high compensation temperature ( $\theta_c$ ). Values of  $\theta_c$  are between 286 and 295 K, *i.e.* the highest among

the rare-earth garnets.<sup>1–3</sup> For practical applications, obtaining materials with  $\theta_c$  near room temperature is essential. All functional key spintronic characteristics, including the magneto-electric or magneto-optic control of the garnet systems are optimal around  $\theta_c$ , hence understanding of the underlying physics controlling  $\theta_c$  is of paramount importance. Nevertheless, tuning of  $\theta_c$  is challenging. Stoichiometry, crystal structure, specific defects and magnetic aspects are all important in this respect. Moreover, the complex correlations between them have to be considered. A precise control of  $\theta_c$  requires a thorough understanding of how the stoichiometric aspects and atomic arrangements imposing the strength and type of exchange interactions modify the temperature dependent magnetic properties. So far, only a few studies have demonstrated an increase in  $\theta_c$  for  $\text{Gd}_3\text{Fe}_5\text{O}_{12}$  and  $\text{Tb}_3\text{Fe}_5\text{O}_{12}$  films by incorporating rare-earth in excess.<sup>4–9</sup> A recent theoretical study has shown that  $\theta_c$  of stoichiometric  $\text{Gd}_3\text{Fe}_5\text{O}_{12}$  could be increased by decreasing the distance between cations, thereby strengthening exchange interactions.<sup>8</sup> According to authors of ref. 10 in  $\text{Tb}_3\text{Fe}_5\text{O}_{12}$  films with Tb deficiency,  $\theta_c$  is independent of the Tb/Fe ratio. Presented information emphasize the lack of a clear understanding concerning the role of chemical composition and atomic site occupation on compensation temperature, be it in stoichiometric or non-stoichiometric materials.

In this study we propose a detailed analysis of the stoichiometry and cations arrangement in  $\text{Gd}_3\text{Fe}_5\text{O}_{12}$  ferrimagnetic garnets synthesized by two different methods. The local atomic configuration is determined with unprecedented accuracy by using three complementary investigation techniques. The aim is to investigate changes in the atomic configuration due to internal substitutions (cationic inversions) when materials are obtained by different processing conditions. Next, the work pioneers understanding of systematic and refined connection between structural details *versus* magnetic functionality with a focus on spintronic  $\theta_c$ . Surprisingly, a small change in atomic arrangement produces a high variation in  $\theta_c$  of up to 27 K. It is

National Institute of Materials Physics, Atomistilor Street 405A, 077125, Magurele, Romania. E-mail: kuncser@infim.ro, badica2003@yahoo.com, petre.badica@infim.ro



noteworthy that  $\theta_c$  variation is conveniently positioned in the room temperature range, thus enabling a high practical potential. By integrating X-ray diffraction analysis and advanced characterization techniques such as magnetometry and Mössbauer spectroscopy, for a precise determination of site occupancy, as well as of material design through innovative processing, this study fills the critical knowledge gap. Our approach not only provides a fundamental perspective for understanding the factors governing  $\theta_c$ , but also provides a new way for the development of personalized customizable materials, thus significantly impacting the design of cutting-edge spintronics technologies. This work also assesses functionality of polycrystalline bulk garnets as useful and interesting items *versus* their thin films, single crystal and nano objects counterparts.

## 2. Experimental

The first garnet sample was obtained by a novel and original route which combines a cost-effective and simple surfactant-assisted hydrothermal synthesis of a mesoporous  $\text{Gd}_3\text{Fe}_5\text{O}_{12}$  nano-powder, followed by sintering.<sup>11</sup> Second sample was prepared by a conventional solid-state reaction method. Namely, a stoichiometric mixture of  $\text{Gd}_2\text{O}_3$  (Fluka, purity > 99.9%) and  $\text{Fe}_2\text{O}_3$  (Fluka, purity > 97%) powders was manually homogenized in an agate mortar. The powder mixture was pressed under  $\sim 5 \text{ kN m}^{-2}$  into a disk of 4 mm diameter. The resulting green compact was sintered in air at  $1400^\circ\text{C}$  for a dwell time of 10 hours. Heating and cooling rates were  $5^\circ\text{C min}^{-1}$ , being selected based on results from ref. 12.

X-ray diffraction spectra were acquired at room temperature with a Bruker-AXS D8 ADVANCE diffractometer ( $\text{CuK}\alpha_1$  radiation,  $\lambda = 1.5406 \text{ \AA}$ ). The ICDD Powder Diffraction database was used for phase identification.<sup>13</sup> Rietveld analysis of the data was performed with MAUD (materials analysis using diffraction) software version 2.98. The background in XRD patterns from Fig. 1 was subtracted from experimental and fitted curves. Local magnetic configurations were investigated by temperature dependent Mössbauer spectroscopy with a conventional

constant acceleration spectrometer (SEECO, USA) that uses a  $^{57}\text{Co}$  (Rh matrix) source. Measurements were performed at six different temperatures (6 K, 50 K, 100 K, 200 K and 300 K) and NORMOS software<sup>14</sup> was employed to fit Mössbauer spectra. Zero-field cooling (ZFC) and field-cooling (FC) curves were measured under an applied field of 300 Oe intensity with a DynaCool PPMS-9T (Quantum Design, USA) magnetometer, in the range from 50 K (*i.e.* magnetic frozen state) to 400 K (*i.e.* with relaxed magnetic moments of Gd ions). Hysteresis loops were obtained at different temperatures in fields of up to 5 T induction *via* the same device. Transmission Electron Microscopy (TEM) investigations were carried out with the JEOL 2100 instrument, equipped with an energy-dispersive X-Ray detector (Japan).

## 3. Results and discussion

Fig. 1(a) and (b) shows the room temperature (RT) XRD patterns of the two  $\text{Gd}_3\text{Fe}_5\text{O}_{12}$  samples. The diffraction peaks of both samples correspond to the phase structure of  $\text{Gd}_3\text{Fe}_5\text{O}_{12}$  (ICDD no. 04-007-521). The parameters obtained from the Rietveld analysis are listed in Table 1. The average crystallite sizes are in the range of  $119 \div 164 \text{ nm}$ . Such values prove a good crystallinity of both garnets, being one order of magnitude higher than specific nanosizes where magnetic and structural properties might be size dependent. From this point of view, the observed differences in the magnetic properties, specifically in the compensation temperatures cannot be related to differences of crystallite size in the indicated interval. Stoichiometric  $\text{Gd}_3\text{Fe}_5\text{O}_{12}$  has a cubic structure in which each  $\text{Gd}^{3+}$  ion is surrounded by 8 oxygen ions, thus forming an inverted dodecahedron.  $\text{Fe}^{3+}$  ions are surrounded either by 6 oxygen ions in specific octahedral ( $\text{Fe}_{\text{oct}}$ ) positions or by 4 oxygen ions in specific tetrahedral ( $\text{Fe}_{\text{tet}}$ ) positions. Oxygen ions are arranged in a 3D lattice and they contribute to stability of the crystal structure. Summarizing, 24 dodecahedral  $\text{Gd}^{3+}$  ions {24c}, 16 octahedral  $\text{Fe}^{3+}$  ions [16a] and 24 tetrahedral  $\text{Fe}^{3+}$  ions (24d) are present in each unit cell.<sup>15</sup>

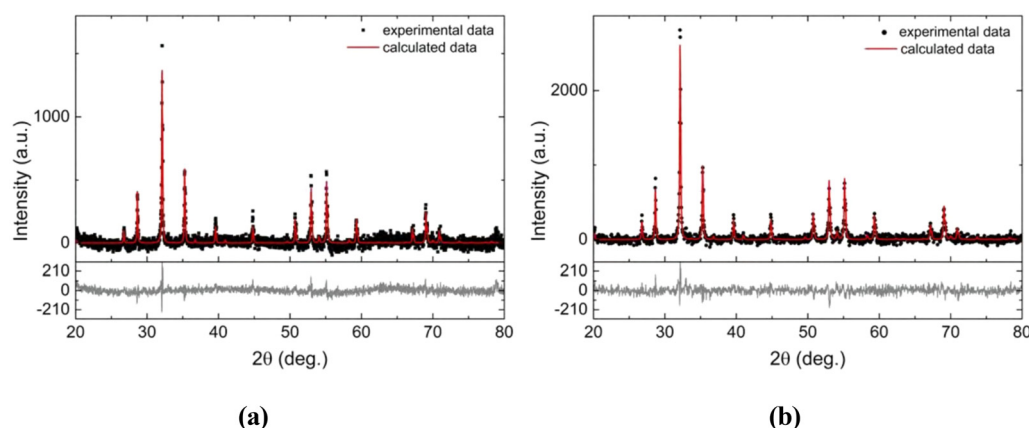


Fig. 1 XRD patterns and Rietveld refinement of  $\text{Gd}_3\text{Fe}_5\text{O}_{12}$  samples prepared by: (a) hydrothermal method; (b) solid state reaction.



**Table 1** Structural parameters obtained from Rietveld refinement: lattice parameter  $a$ , crystallite size ( $D_{\text{eff}}$ ), lattice micro strain  $\langle \epsilon^2 \rangle^{1/2}$ , the calculated  $R$ -factor,  $R_{\text{exp}}$ , and  $\chi^2$  factor. The resulted optimal site occupation respecting also the Mössbauer spectroscopy investigation is also mentioned, with an error of less than 3 units at the last digit

| Samples  |   |
|--|---|
| Gd <sub>3</sub> Fe <sub>5</sub> O <sub>12</sub> obtained by hydrothermal method (see Fig. 1a)  | (Gd <sub>2.40</sub> Fe <sub>0.30</sub> )(Fe <sub>1.46</sub> Gd <sub>0.30</sub> )Fe <sub>3</sub> O <sub>11.9</sub><br>$a = 12.457 \pm 3 \times 10^{-4}$ Å<br>$D_{\text{eff}} = 164 \pm 6$ nm<br>$\langle \epsilon^2 \rangle^{1/2} = 1 \times 10^{-4} \pm (<1 \times 10^{-5})$<br>$R_{\text{exp}} (\%) = 4.55$<br>$\chi^2 = 1.91$ |
| Gd <sub>3</sub> Fe <sub>5</sub> O <sub>12</sub> obtained by solid state reaction (see Fig. 1b) | (Gd <sub>2.64</sub> Fe <sub>0.36</sub> )(Fe <sub>1.32</sub> Gd <sub>0.32</sub> )Fe <sub>3</sub> O <sub>11.5</sub><br>$a = 12.457 \pm 3 \times 10^{-4}$ Å<br>$D_{\text{eff}} = 119 \pm 3$ nm<br>$\langle \epsilon^2 \rangle^{1/2} = 1 \times 10^{-4} \pm (<1 \times 10^{-5})$<br>$R_{\text{exp}} (\%) = 3.44$<br>$\chi^2 = 1.45$ |

However, the Rietveld analysis gives clear indication for the formation of non-stoichiometric cubic structures for both materials.

Accordingly, to accommodate the observed non-stoichiometry it was necessary to consider cation inversions occurring between Gd<sup>3+</sup> and Fe<sup>3+</sup> ions at the octahedral positions. As presented in the following, the chemical formulas which are in simultaneous agreement with both Rietveld and Mössbauer analyses are (Gd<sub>2.40</sub>Fe<sub>0.30</sub>)(Fe<sub>1.46</sub>Gd<sub>0.30</sub>)Fe<sub>3</sub>O<sub>11.9</sub> and (Gd<sub>2.64</sub>Fe<sub>0.36</sub>)(Fe<sub>1.32</sub>Gd<sub>0.32</sub>)Fe<sub>3</sub>O<sub>11.5</sub> for samples prepared by hydrothermal and solid-state routes, respectively. The amounts of ions involved in the inversion are very close for both materials, being approximately 6% (atomic percent) for Fe<sup>3+</sup> and about 10% (atomic percent) for Gd<sup>3+</sup>. Both samples have a deficit of cations, *e.g.* 0.3 Gd<sup>3+</sup>, 0.24 Fe<sup>3+</sup> and 0.04 Gd<sup>3+</sup>, 0.32 Fe<sup>3+</sup> atoms for Gd<sub>3</sub>Fe<sub>5</sub>O<sub>12</sub> synthesized by hydrothermal and solid-state reaction routes, respectively. The impact of these inversions and of the deficient of Gd<sup>3+</sup> cations is also reflected in the lattice constant values, which exhibit a slight decrease ( $a = 12.457$  Å in both samples), comparative to the theoretical values of 12.470 Å for the stoichiometric compound,<sup>13</sup> thus confirming slight distortions of the two crystal lattices.

The temperature dependent Mössbauer spectra of the two Gd<sub>3</sub>Fe<sub>5</sub>O<sub>12</sub> samples are shown in Fig. 2(a) and (b). They have been fitted with three sextets, characterized by the following hyperfine parameters: hyperfine magnetic field ( $B_{\text{hf}}$ ), isomer shift (IS) and quadrupolar shift ( $\epsilon$ ). Their values obtained from the spectral analysis (without any fit constrain) are presented in Table 2. The correlated values of IS and  $\epsilon$  provide information on the local electronic structure including valence state of Fe ions on each site as well as on their oxygen coordination whereas the hyperfine magnetic field is the main parameter providing information on the magnetic structure, being proportional in magnitude with the electronic magnetic moment of the Fe ions.

The assignation of the two main Mössbauer components (the first and the third spectral component in the above table below 100 K) have been done in agreement with values of hyperfine parameters reported in literature for spectra of Gd<sub>3</sub>Fe<sub>5</sub>O<sub>12</sub> samples with garnet oxide structures.<sup>16,17</sup> Note that

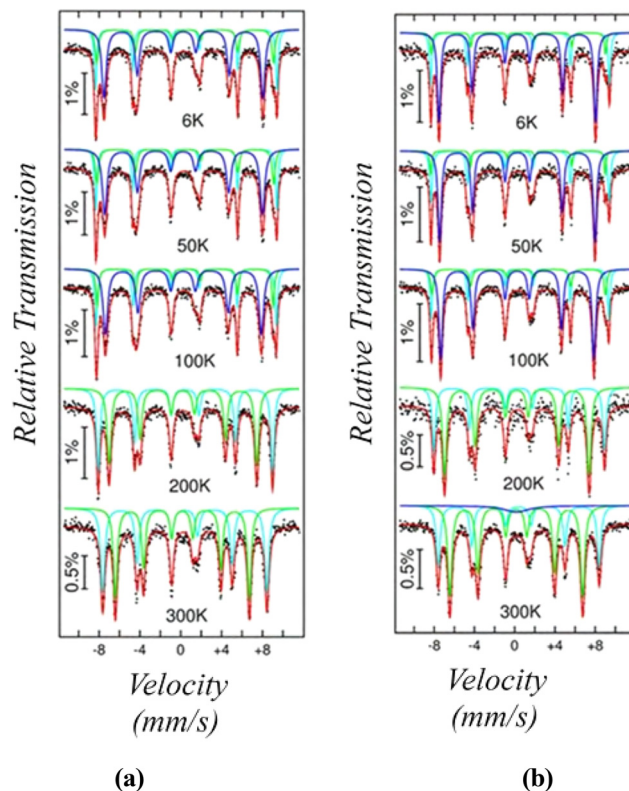


**Fig. 2** Mössbauer spectra of Gd<sub>3</sub>Fe<sub>5</sub>O<sub>12</sub> samples prepared by: (a) hydrothermal method; (b) solid state reaction.

a realistic site occupancy of Fe ions can be subtracted only from the spectra at low temperature, while at higher temperatures (*i.e.* above 100 K) magnetic relaxation phenomena appear with an influence on the time average value of the magnetic moment of Fe, leading implicitly to a different decreasing trend of the hyperfine field in each position. For example, above 200 K, there is a superposition of the hyperfine magnetic fields of the first two sextets leading to only two spectral components in the fit. However, the hyperfine magnetic field of the third sextet decreases much faster than for the first two, giving evidence for a much faster magnetic relaxation of the magnetic moment associated to this Fe position. At 6 and 50 K, the sextet with an IS of about 0.39 mm s<sup>-1</sup> and with the highest hyperfine magnetic field of about 55 T was assigned to Fe<sup>3+</sup> ions in the high-spin state on the octahedral positions in the garnet, whereas the sextet with an IS of about 0.17 mm s<sup>-1</sup> and with the lowest hyperfine magnetic field of about 48 T was assigned to Fe<sup>3+</sup> ions in the high-spin state on the tetrahedral positions.<sup>16</sup> Neglectable values of  $\epsilon$  are specific to these positions. Finally, the third (less intense) sextet with the highest value of IS of about 0.43 mm s<sup>-1</sup> and an intermediate value of the hyperfine magnetic field of about 54 T was assigned to Fe<sup>3+</sup> ions which occupy the dodecahedral positions of Gd<sup>3+</sup> ions in the garnet. One of the reasons for this assignation is the reported trend of IS value with the number of oxygen ions around the cation.<sup>16</sup> In addition, the relative number of Fe<sup>3+</sup> cations on this position, (*i.e.* of only 9% relative spectral area) is



**Table 2** The magnetic hyperfine parameters ( $B_{\text{hf}}$ , IS,  $\varepsilon$ ) obtained by fitting the Mössbauer spectra from Fig. 2. The spectral linewidth,  $\Gamma$ , as well as the relative spectral area of the three components (evidenced at lower temperatures, *i.e.* where magnetic relaxation phenomena can be neglected) are also presented. IS is given relative to  $\alpha$ -Fe at RT. Errors are of one unit at the last-mentioned digit, except for the relative spectral area where the errors are of 5 units of the last digit. At temperatures higher than 200 K, only two sextets components were used due to enhanced relaxation phenomena, pointed also by the broad central pattern improving the fit at 300 K (Fig. 2(b))

| $T$ (K) | Gd <sub>3</sub> Fe <sub>5</sub> O <sub>12</sub> obtained by hydrothermal method |                          |                                     |                                |          | Gd <sub>3</sub> Fe <sub>5</sub> O <sub>12</sub> obtained by solid state reaction |                          |                                     |                                |                   |
|---------|---|--------------------------|-------------------------------------|--------------------------------|----------|--|--------------------------|-------------------------------------|--------------------------------|-------------------|
|         | $B_{\text{hf}}$ (T)   | IS (mm s <sup>-1</sup> ) | $\varepsilon$ (mm s <sup>-1</sup> ) | $\Gamma$ (mm s <sup>-1</sup> ) | Area (%) | $B_{\text{hf}}$ (T)  | IS (mm s <sup>-1</sup> ) | $\varepsilon$ (mm s <sup>-1</sup> ) | $\Gamma$ (mm s <sup>-1</sup> ) | Area (%)          |
| 6       | 55.40   | 0.39                     | 0.10                                | 0.31                           | 31.2     | 55.09  | 0.38                     | 0.12                                | 0.28                           | 25.9              |
|         | 53.80   | 0.43                     | -0.31                               | 0.29                           | 9.2      | 53.63  | 0.42                     | -0.29                               | 0.40                           | 10.1              |
|         | 48.55   | 0.16                     | -0.01                               | 0.38                           | 59.6     | 48.24  | 0.16                     | -0.00                               | 0.32                           | 64.1              |
| 50      | 55.33   | 0.39                     | 0.09                                | 0.31                           | 29.9     | 54.87  | 0.39                     | 0.12                                | 0.32                           | 27.5              |
|         | 53.81   | 0.42                     | -0.27                               | 0.27                           | 9.0      | 53.73  | 0.39                     | -0.31                               | 0.22                           | 9.0               |
|         | 48.18   | 0.17                     | -0.00                               | 0.43                           | 61.1     | 47.86  | 0.17                     | -0.00                               | 0.40                           | 63.5              |
| 100     | 55.09   | 0.38                     | 0.09                                | 0.31                           | 28.8     | 54.71  | 0.38                     | 0.10                                | 0.27                           | 21.3              |
|         | 53.77   | 0.42                     | -0.23                               | 0.26                           | 9.2      | 53.37  | 0.41                     | -0.20                               | 0.36                           | 15.2              |
|         | 47.61   | 0.16                     | 0.01                                | 0.47                           | 62.0     | 47.26  | 0.16                     | 0.02                                | 0.43                           | 63.5              |
| 200     | 53.24   | 0.34                     | 0.05                                | 0.38                           | 41.3     | 52.63  | 0.34                     | 0.03                                | 0.41                           | 37.4              |
|         | 45.03   | 0.11                     | 0.01                                | 0.43                           | 58.7     | 44.55  | 0.12                     | -0.00                               | 0.49                           | 62.6              |
| 300     | 50.05   | 0.28                     | 0.04                                | 0.40                           | 42.8     | 49.62  | 0.29                     | 0.03                                | 0.46                           | 34.9              |
|         | 41.27   | 0.06                     | -0.01                               | 0.39                           | 57.2     | 40.95  | 0.06                     | 0.00                                | 0.45                           | 59.0 <sup>a</sup> |

<sup>a</sup> The relative areas of the central component was not counted.

in good agreement with the Rietveld analysis. However, the higher distortion of this position, underlined by the significant value of  $\varepsilon$  of about  $-0.3 \text{ mm s}^{-1}$ , suggests rather a deficient number of surrounding oxygen anions in this configuration (*i.e.* 7 instead of 8). The relative areas at low temperatures in Table 2 are in agreement with a population of 30% of the octahedral positions and 61% of the tetrahedral positions of Fe in the garnet obtained by the hydrothermal method and of 27% of the octahedral positions and 63% of tetrahedral positions of Fe in the garnet obtained by the solid-state method (close to 10% of Fe ions are on the Gd positions) in good agreement with the best compositional solution of the Rietveld analysis, previously presented. For example, the above results show clearly a ratio of tetrahedral to octahedral Fe positions higher than the theoretical value of 3/2, meaning that the tetrahedrally coordinated Fe positions are not affected by inversion, but only the octahedrally coordinated ones. Moreover, the estimated occupancy of the octahedral Fe positions per formula unit is 31/60 multiplied by 3 (theoretical number of Fe atoms with tetrahedral occupation), leading to 1.47 Fe ions with octahedral coordination in case of sample obtained by the hydrothermal method. In a similar way, a value of 1.29 Fe ions with octahedral coordination is estimated in case of sample obtained by solid-state method.

Based on Mössbauer data, the effective magnetic moments of the Fe<sup>3+</sup> ions at different temperatures can be computed on each position by assuming a proportionality constant of 11 T/ $\mu_B$  between the magnetic moment and the hyperfine magnetic field.<sup>18</sup> Noteworthy is that the magnetic structure of Gd<sub>3</sub>Fe<sub>5</sub>O<sub>12</sub> shows antiferromagnetic coupling between the two sublattices of Fe<sup>3+</sup> ions (octahedral and tetrahedral), while the rare earth ions are ferromagnetically coupled to the Fe<sup>3+</sup> ions in the octahedral position.<sup>19</sup> Under this assumption and considering Gd<sup>3+</sup> ions with a magnetic moment of  $7\mu_B$ ,<sup>15</sup> the magnetic moments per formula units (in  $\mu_B$ ) were calculated for both samples at low temperatures where magnetic relaxation effects

are negligible. The magnetic structure presented in SI was considered, with weighted contributions of the atomic magnetic moments, according to the established ion occupancy, as also mentioned in the above material. The values of magnetic moments per unit formula were  $14.57\mu_B$  for Gd<sub>3</sub>Fe<sub>5</sub>O<sub>12</sub> obtained by hydrothermal method and  $15.98\mu_B$  for Gd<sub>3</sub>Fe<sub>5</sub>O<sub>12</sub> synthesized by solid state reaction. Both magnetic moments are smaller than the theoretical value of  $16\mu_B$ , but they are consistent with the structures (chemical composition and atoms positions, Table 1) determined through Rietveld analysis.

Hysteresis loops at different temperatures for both samples are presented in Fig. 3. As a result of the complex type of coupling inside the unit cell of the garnet, the magnetic properties are highly sensitive to local changes. Both the cation distribution and defects arising from variations in oxygen stoichiometry are crucial factors in understanding the evolution of these properties. Both samples exhibit significant ferrimagnetic behavior at low temperatures. As the temperature increases up to 300 K, the saturation magnetization values decrease rapidly, due to thermal fluctuations that change the effective magnetic moments and coupling strength. The saturation magnetization values at low temperatures (5 K) are consistent with those reported in previous studies,<sup>20</sup> *i.e.*  $94.5 \text{ emu g}^{-1}$  for Gd<sub>3</sub>Fe<sub>5</sub>O<sub>12</sub> synthesized *via* solid-state reaction and  $90.15 \text{ emu g}^{-1}$  for Gd<sub>3</sub>Fe<sub>5</sub>O<sub>12</sub> obtained by the hydrothermal method. Again, the corresponding magnetic moments calculated for both samples are in good agreement with those calculated from the Mössbauer data, *i.e.*  $15.46\mu_B$  for the solid-state reaction sample and  $14.08\mu_B$  for the hydrothermal sample.

The magnetization curves measured in ZFC and FC conditions as a function of temperature under an applied magnetic field of 300 Oe, are shown in Fig. 4.

Both ZFC-FC curves show a relatively high magnetization at low temperatures where magnetic ordering of Gd<sup>3+</sup> sublattice occurs.<sup>21</sup> The compensation temperatures vary considerably.





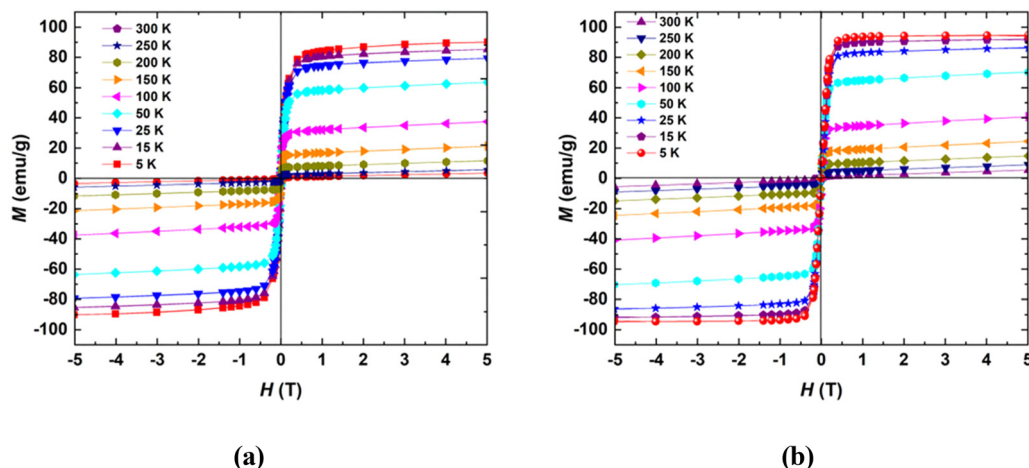


Fig. 3 Hysteresis loops acquired at different temperatures for  $\text{Gd}_3\text{Fe}_5\text{O}_{12}$  samples prepared by: (a) hydrothermal method; (b) solid state reaction.

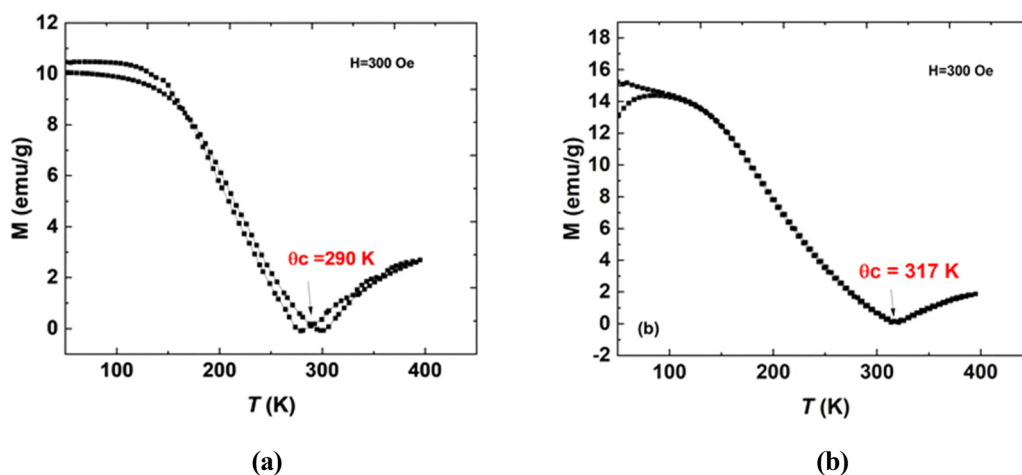


Fig. 4 ZFC-FC curves measured in an applied magnetic field for  $\text{Gd}_3\text{Fe}_5\text{O}_{12}$  prepared by: (a) hydrothermal method; (b) solid state reaction.

The  $\text{Gd}_3\text{Fe}_5\text{O}_{12}$  synthesized by hydrothermal method has a  $\theta_c$  of 290 K. The garnet produced through the solid-state reaction exhibits a 27 K increase in  $\theta_c$  due to a higher occupancy of the dodecahedral Gd positions and consequently stronger Fe–Gd interactions. That can be straightforward understood by the mechanism of the compensation temperature. The compensation is realized when the diminished time average magnetic moment of Gd ions, *via* temperature activated magnetic relaxation, equates the time average magnetic moment of the opposite magnetic sublattice, due to mainly Fe ions. The relaxation of Gd magnetic moment increases faster with temperature if the stronger Gd–Fe interactions are replaced by the weaker Gd–Gd interactions. This is achieved for a higher occupation of dodecahedral Gd positions by Fe atoms while the number of Gd cation neighbors of a Gd ion is higher in this case (see SI with magnetic structure). Accordingly, a higher compensation temperature is expected in case of the structure with less Fe ions on the Gd position (*i.e.* for the sample obtained by solid state reaction) as compared to the case of a garnet with higher

occupation of Gd positions by Fe ions (*i.e.* for sample obtained by the hydrothermal method).

## 4. Conclusions

Current understanding<sup>22</sup> is that compensation temperature is influenced by three main factors: (i) the nature of the rare earth ion, which has specific values of magnetic moments; (ii) the exchange interactions between iron and the rare earth elements; and (iii) substitutions and doping. In addition to these factors, our results demonstrate that internal substitutions through cation inversions in which iron ions from the octahedral sites migrate to the gadolinium positions and *vice versa* are of paramount importance and also show the strongest dependence on preparation methods. Therefore, even for a fixed stoichiometry, due to different atomic arrangements leading to a different distribution of Fe–Fe and Fe–Gd magnetic couplings, compensation temperature changes significantly and this takes place in the room temperature range. The impact is



remarkably high, promoting extended possibilities of designing garnet systems with controllable compensation temperatures. This in turn enables customizable advanced spintronic applications with *e.g.* fast magneto-optical switching and magneto-electric control.

The stoichiometric and site occupancy details for both materials obtained by different processing routes were established with high precision through the proposed extensive methodology. The proposed approach opens new directions for enhancement of materials with tailored magnetic functionalities.

## Author contributions

Cristina Bartha: writing – original draft, supervision, investigation, funding acquisition, conceptualization, formal analysis, Claudiu Locovei: visualization, formal analysis, Andrei Alexandru-Dinu: visualization, data acquisitions, Cezar Comanescu: processing, visualisation, Mihai Alexandru Grigorescu: processing, visualization, data acquisitions, Andrei Kuncser: data acquisitions, formal analysis, Nicusor Iacob: data acquisitions, Magda Galatanu: data acquisitions, Aurel Leca: data acquisitions, Petre Badica: writing – review & editing, conceptualization, supervision, formal analysis, validation, Victor Kuncser: writing – original draft, supervision, validation, investigation, conceptualization.

## Conflicts of interest

There are no conflicts to declare.

## Data availability

Data supporting the results of this study can be obtained from the corresponding author upon request.

Supplementary information is available. See DOI: <https://doi.org/10.1039/d5cp02696b>.

## Acknowledgements

Authors acknowledge support from UEFISCDI through projects: PN-III-P2-2.1-PED-2021-2007 (contract no. 676PED/2022), PN-IV-P7-7.1 PED (contract no 63 PED/2025), and Core Programs PC1-PN23080101 and PC2-PN23080202.

## References

- 1 P. G. Li, S. G. Ng, X. Yuan, F. X. Zhang, H. F. Wong, Z. Q. Chu, P. Cao and C. W. Leung, Spin magnetotransport in rare-earth iron garnet (REIG)/Pt: Effects of modulated bulk and REIG/Pt interfaces, *APL Mater.*, 2024, **12**, 081114.
- 2 N. Aparnadevi, K. S. Kumar, M. Manikandan, B. S. Kumar, J. S. Punitha and C. Venkateswaran, Structural properties, optical, electrical and magnetic behavior of bismuth doped  $\text{Gd}_3\text{Fe}_5\text{O}_{12}$  prototype garnet, *J. Mater. Sci.: Mater. Electron.*, 2020, **31**, 2081.
- 3 C. Holzmann, A. Ullrich, O. T. Ciubotariu and M. Albrecht, Stress-Induced Magnetic Properties of Gadolinium Iron Garnet Nanoscale-Thin Films: Implications for Spintronic Devices, *ACS Appl. Nano Mater.*, 2022, **5**, 1023.
- 4 M. Oron, I. Barlow and W. F. Traber, Ferrimagnetic garnet thin films: Growth, structure and some magnetic properties, *J. Mater. Sci.*, 1969, **4**, 271.
- 5 E. Sawatzky and E. Kay, Magnetic and Structural Properties of Epitaxial and Polycrystalline GdIG Films Prepared by rf Sputtering, *J. Appl. Phys.*, 1971, **42**, 367.
- 6 E. R. Rosenberg, L. B. Avci, C. Zeledon, B. Song, C. Gonzalez-Fuentes, J. Mendil, P. Gambardella, M. Veis, C. Garcia, G. S. D. Beach and C. A. Ross, Magnetism and spin transport in rare-earth-rich epitaxial terbium and europium iron garnet films, *Phys. Rev. Mater.*, 2018, **2**, 094405.
- 7 Z. Ren, K. Qian, M. Aldosary, Y. Liu, S. K. Cheung, I. Ng, J. Shi and Q. Shao, Strongly heat-assisted spin-orbit torque switching of a ferrimagnetic insulator, *APL Mater.*, 2021, **9**, 051117.
- 8 T. Bayarara, C. Xu, D. Campbell and L. Bellaiche, Tuning magnetization compensation and Curie temperatures in epitaxial rare earth iron garnet films, *Phys. Rev. B*, 2019, **100**, 214412.
- 9 P. Wang, J. Ke, G. S. Li, L. Z. Bi, C. Hu, Z. Zhu, J. Liu, Y. Zhang and J. W. Cai, Tuning magnetization compensation temperature of  $\text{Gd}_3\text{Fe}_5\text{O}_{12}$  epitaxially grown on  $\text{Gd}_3\text{Sc}_2\text{Ga}_3\text{O}_{12}$ , *Appl. Phys. Lett.*, 2024, **124**(17), 172405.
- 10 S. Damerio and C. O. Avci, Sputtered terbium iron garnet films with perpendicular magnetic anisotropy for spintronic applications, *J. Appl. Phys.*, 2023, **133**, 073902.
- 11 C. Bartha, C. Comanescu, A. Alexandru-Dinu, M. A. Grigorescu, A. Kuncser, P. Badica and V. Kuncser, Obtaining oxide materials in form of mesoporous nanopowders with garnet structure based on iron and rare earths used in *e.g.* sensors by modified hydrothermal of non-ionic surfactant of triblock copolymer of polyoxypropylene (propylene oxide), Patent request number RO137656-A0.
- 12 A. N. Hapishah, M. N. Hamidon, M. M. Syazwan and F. N. Shafiee, Effect of grain size on microstructural and magnetic properties of holmium substituted yttrium iron garnets ( $\text{Y}_{1.5}\text{Ho}_{1.5}\text{Fe}_5\text{O}_{12}$ ), *Results Phys.*, 2019, **14**, 102391.
- 13 PDF-ICDD. Powder Diffraction File (PDF-4+ 2022 Software 4.22.0.2), International Centre for Diffraction Data: Newtown Square, 2011, PA, USA.
- 14 R. A. Brand, Improving the validity of hyperfine field distributions from magnetic alloys, Part I: Unpolarized source, *Nucl. Instrum. Methods Phys. Res., Sect. B*, 1987, **28**, 398.
- 15 S. Geller, Crystal chemistry of the garnets, *Zeitschrift für Kristallographie, Cryst. Mater.*, 1967, **125**(1), 1–6.
- 16 J. C. Waerenborgh, D. P. Rojas, A. L. Shaula, V. V. Kharton and F. M. B. Marques, Defect formation in  $\text{Gd}_3\text{Fe}_5\text{O}_{12}$ -based garnets: a Mössbauer spectroscopy study, *Mater. Lett.*, 2004, **58**, 3432.
- 17 M. Kuila and V. R. Reddy, In-field  $^{57}\text{Fe}$  Mössbauer spectroscopy study of polycrystalline rare-earth iron garnet



- ( $R_3Fe_5O_{12}$ ;  $R = Y, Gd, Ho, Tm, \& Yb$ ) compounds, *Hyperfine Interact.*, 2021, **242**, 36.
- 18 T. E. Cranshaw and G. Longworth, in Mössbauer Spectroscopy of Magnetic Systems, *Mössbauer Spectroscopy Applied to Inorganic Chemistry*, ed. G. J. Long, Modern Inorganic Chemistry, 1984, 1.
  - 19 W. Liu, B. Cheng, S. Ren, W. Huang, J. Xie, G. Zhou, H. Qin and J. Hu, Thermally assisted Magnetization Control and Switching of  $Dy_3Fe_5O_{12}$  and  $Tb_3Fe_5O_{12}$ , Ferrimagnetic Garnet by Low Density Current, *J. Magn. Magn. Mater.*, 2020, **507**, 166804.
  - 20 J. Sultana, J. Mohapatra, P. J. Liu and S. R. Mishra, Structural, magnetic, and magnetocaloric properties of chromium doped  $Gd_3Fe_{5-x}Cr_xO_{12}$  garnet compound, *AIP Adv.*, 2023, **13**, 025252.
  - 21 R. Z. Levitin, V. V. Snegirev, A. V. Kopylov, A. S. Lagutin and A. Gerber, Magnetic method of magnetocaloric effect determination in high pulsed magnetic fields, *J. Magn. Magn. Mater.*, 1997, **170**, 223.
  - 22 P. W. Anderson, Theory of Magnetic Exchange Interactions: Exchange in Insulators and Semiconductors, *Solid State Phys.*, 1963, **14**, 99.

